

stages, a five-turn helix comes within 90 percent of reversible contraction (T_*).

Operation is made continuous by forming the fiber into a closed loop and disposing the spindles and water bath so that the fiber loop passes from one bath to the other.

The maximum mechanical work that can be obtained from collagen fiber moving through the 1-2-3-1 cycle is the area enclosed by the ideal cycle on the tension-length plane (Fig. 1). For fibers having a specific length (dry) of 270 cm/g and a density of 1.3 g/cm³, this area (maximum or reversible work) is 7.85×10^6 erg per gram of fiber. Consequently a turbine, such as that shown in the Fig. 4 photograph, which has a collagen throughput of 0.09 g/sec, has a maximum or ideal power output of 70 mw. Our actual turbine has delivered about 30 mw, corresponding to a mechanical efficiency of 40 percent.

Free energy conversion efficiency (ratio of work output to free energy of dilution of the salt solutions consumed) is at present considerably smaller (> 1 percent) than the mechanical efficiency, because relatively large quantities of salt solution and wash water cling to the fiber surface and are mechanically carried from one bath into the other, mixing without contributing to the engine output. This deficiency can probably be reduced by incorporating fiber-wiping devices in the cycle.

The work output per cycle can be augmented if the water-washed fiber is slightly elongated (pretensioned) before immersion in salt solution, as shown by the cycle 1-1a-1b-2-3-1 (Fig. 1). Pretensioning is achieved by placing short inverted conical sections immediately above the cylindrical portions of the turbine spindles. Collagen working fiber can also be fueled with CaCl₂, MgCl₂, KSCN, and other aqueous solutions. We have in fact operated the turbine in brine taken directly from the Dead Sea.

The turbine and power cycles described here may be employed with any linearly disposed contractile material which undergoes an appreciable reversible shrinkage or tension increase (or both) when subjected to a change in its environmental potential. The environmental change may be other than chemical. For example, a thermally powered contraction turbine can be operated with linear crystalline polyethylene or rubber working fibers, provided that a heat bath replaces the salt bath and a cooling zone replaces the water regenerating bath.

It is thermodynamically possible to

operate all of these cycles backward as pumps so that the foregoing thermal engine would function as a refrigerator or air conditioner which uses an elastomeric refrigerant.

M. V. SUSSMAN*

A. KATCHALSKY

Polymer Department, Weizmann
Institute of Science, Rehovot, Israel

References and Notes

1. A. Katchalsky, I. Steinberg, A. Oplatka, A. Kam, U.S. Patent No. 3,321,908, 30 May 1967; I. Steinberg, A. Oplatka, A. Katchalsky, *Nature* **210**, 568 (1966).
 2. The collagen fiber, manufactured by Ethicon Corp., Somerville, N.J., is cross-linked by treatment with 0.5 percent formaldehyde before it is used.
 3. M. Levy, unpublished data on the force-length dependence of collagen fiber after repeated contractions and expansions.
 4. Supported by NIH special research fellowship 1F3-GM-36,897-01 (to M.V.S.).
- * On leave from the Department of Chemical Engineering, Tufts University, Medford, Mass.
- 3 June 1969; revised 22 August 1969

Evidence for Solid Carbon Dioxide in the Upper Atmosphere of Mars

Abstract. *The infrared spectra recorded by Mariner 6 and 7 show reflections at 4.3 microns, which suggest the presence of solid carbon dioxide in the upper atmosphere of Mars.*

In each of the Mariner 6 and 7 missions to Mars (1), the infrared spectrometer (2) recorded spectra in the 4- μ region as the field of view passed through the atmosphere on the bright limb of the planet. This occurred three times and each time a reflection spike was recorded at 2346 ± 10 cm⁻¹, at the center of the ν_3 absorption band of CO₂. No such reflection was observed in either of two dark limb crossings. Figure 1 shows the three bright limb observations. Figure 2 shows again the second Mariner 7 limb crossing in addition to the spectrum recorded 20 seconds earlier (off the limb) and that recorded 10 seconds later (over the planet). Figure 3 shows a laboratory "reflection-absorption" spec-

trum of 15 μ of annealed solid CO₂ (Matheson) condensed at 77°K on a stainless steel plate that filled the field of view of a flight model spectrometer identical to the Mariner instruments (3). With thicknesses exceeding a few microns, a reflection spike is observed due to the index of refraction variation (4) through the 4.3- μ absorption band of CO₂.

It is clear that the reflection spikes displayed in Fig. 1 are highly characteristic and are attributable to solid CO₂. They are surely not due to solid CO₂ on the planetary surface viewed with stray light from outside the principal field of view of the spectrometer. Local surface temperatures at these latitudes exceed 250°K, much too high to permit condensation on the surface. Furthermore, reflection at 2346 cm⁻¹ from the surface would not be observed because the atmosphere is opaque at this frequency. The reflection must be associated with solid CO₂ at such high altitudes that the atmosphere is no longer optically thick.

Trajectory calculations (5) provide geometrical parameters that help to interpret these observations. Table 1 lists the slant range to the point above which the center of the field of view passes closest to the planet, the latitude and longitude of this point, and the aperture width at this slant range. For the second Mariner 7 limb crossing, it is possible to deduce the time between the reflection spike observation and the limb crossing as 5.5 ± 1.5 seconds. This corresponds to an altitude of the optical path at closest approach of 25 ± 7 km.

If it is assumed that this reflection originates over the field of view's closest approach point, the condensation of CO₂ gives an indication of the temperature at this altitude (T_h). The value of T_h so derived, based on an assumed scale height of 8 km, is 130°K.

There are other infrared absorptions that may also be connected with solid CO₂ in the atmosphere—solid CO₂ ab-

Table 1. Conditions under which reflection at 2346 cm⁻¹ was observed by Mariner 6 and 7 in 1969.

	Mariner 6	Mariner 7	Mariner 7
Date	30 July	4 August	4 August
Time	5:19:07	4:43:23	4:54:55
Latitude	2.5°S	22°N	3°S
Longitude	300°E	343°E	355°E
Local time	Noon	Late morning	Noon
Surface temperature		~250°K	~275°K
Slant range	8180 km	9830 km	6500 km
Aperture width	11 km	17 km	11 km

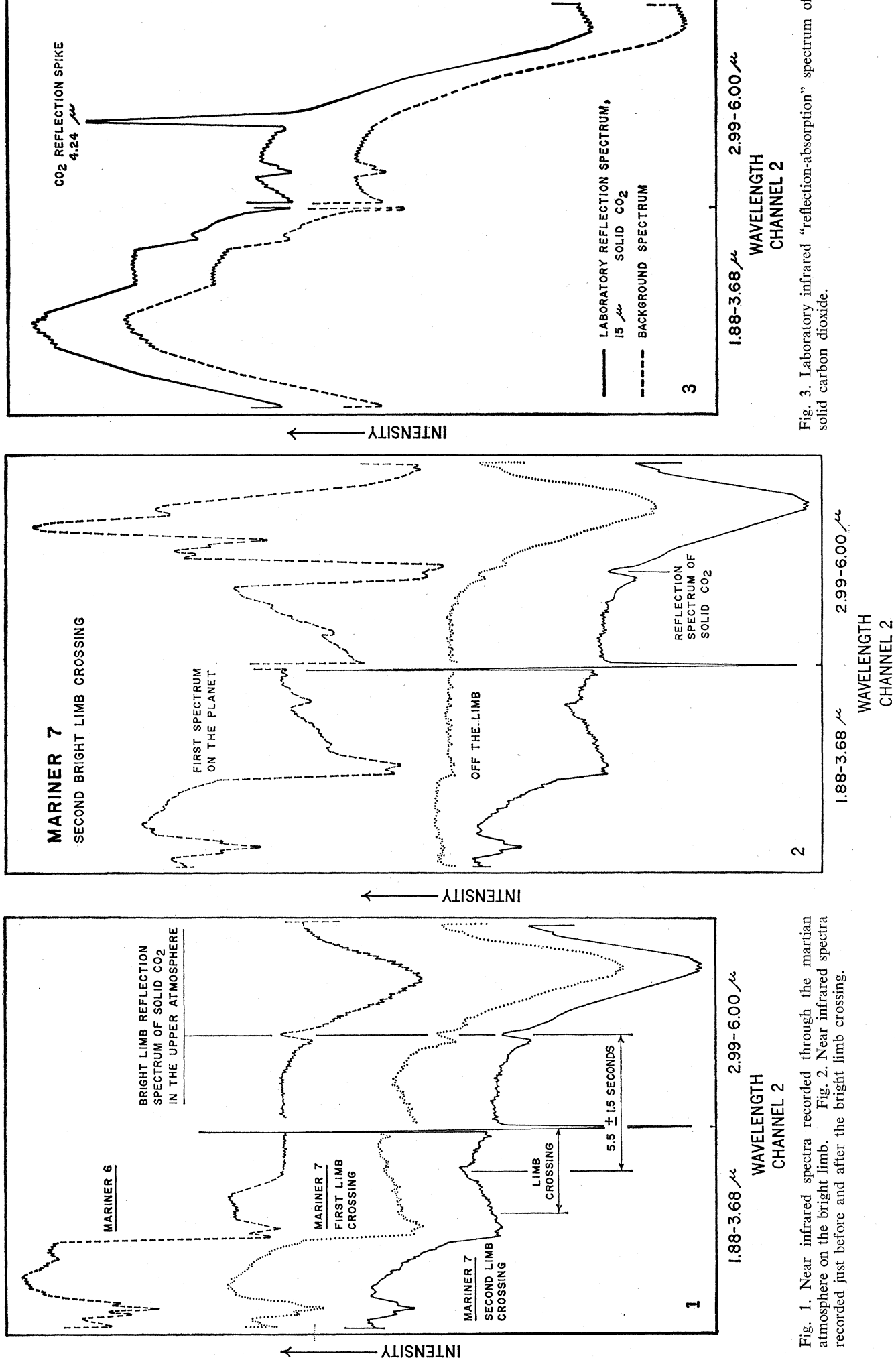


Fig. 3. Laboratory infrared "reflection-absorption" spectrum of solid carbon dioxide.

Fig. 1. Near infrared spectra recorded through the martian atmosphere on the bright limb. Fig. 2. Near infrared spectra recorded just before and after the bright limb crossing.

sorptions at 3μ observed over the polar cap edge (3) and dark limb absorptions near 12μ . The possible relations among these observations are under study.

KENNETH C. HERR
GEORGE C. PIMENTEL

Department of Chemistry and
Space Sciences Laboratory,
University of California, Berkeley

References and Notes

1. Mariner 6 and 7 were NASA missions managed by the Jet Propulsion Laboratory (JPL) and directed by Project Manager H. M. Schurmeier.
2. The spectrometers were designed and con-

structed by the authors in the chemistry department and Space Sciences Laboratory at the University of California, at Berkeley.

3. The manner of illumination and rate of deposition have been described [K. C. Herr and G. C. Pimentel, *Science* **166**, 496 (1969)].
4. Analogous transmission spikes are observed in transmission spectra of molecular solids. They have been observed, for example, for solid carbon monoxide by G. E. Ewing and G. C. Pimentel [*J. Chem. Phys.* **35**, 925 (1961)]; see also G. E. Ewing, thesis, University of California, Berkeley (1960).
5. These trajectory calculations are based on JPL Pegasus calculations made for Mariner 6 after encounter and for Mariner 7 on 8 August 1969. Because the Mariner 7 spacecraft experienced a pre-encounter orbit anomaly, altitudes were inferred from the spectra themselves. All times are Greenwich mean times at the moment of observation of Mars.

10 October 1969

Lunar Igneous Intrusions

Abstract. Photographs taken from Apollo 10 and 11 reveal a number of probable igneous intrusions, including three probable dikes that crosscut the wall and floor of an unnamed 75-kilometer crater on the lunar farside. These intrusions are distinguished by their setting, textures, structures, and brightness relative to the surrounding materials. Recognition of these probable igneous intrusions in the lunar highlands supports the indications of the heterogeneity of lunar materials and the plausibility of intrusive igneous activity, in addition to extrusive volcanism, on the moon.

On the Apollo 10 and 11 missions, a number of regions on the lunar farside were photographed. Previous photographic coverage of these regions was provided by the unmanned Luna and Lunar Orbiter spacecraft. However, the resolution, sun angle, and viewing direction of Apollo photography helped delineate features and structures not evident in previous photography.

One of these regions includes an unnamed (1), generally round, partly crenulated, relatively young, large crater, about 75 km in diameter (Fig. 1). The crater, whose center is at approximately 4°N , 120°E on the Lunar Farside Chart (LFC-1), is situated in as yet undivided highland materials in the general area previously known as the "Soviet Mountains" (2). It exhibits a raised, wavy, and sculptured rim and terraced interior walls which suggest, although not unequivocally, an impact origin. It is not clear from the photographs whether the crater is rayed; the presence of an extensive ray system is held by most as a strong criterion for the impact origin of the younger lunar craters.

The crater is a few kilometers deep, and the depth of its floor in relation to the rim crest varies with the amount of fill. The crater wall is terraced, up to six levels, and the highest terrace is steeper than most, a feature common to craters of similar size. The floor of the

crater displays a prominent central peak that is forked. It forms a unique Y-shape (Figs. 1 and 2), with the right arm trending nearly due north.

Apollo 10 and 11 photographs of this crater are oblique views, taken at high sun illumination with a hand-held Hasselblad camera from an altitude of about 110 km above the lunar surface. On Apollo 10, both the 80-mm lens (frames 4470 to 4474) and the 250-mm lens (frames 4349 to 4364) were used. Similarly, on the Apollo 11 mission the crater was photographed in medium resolution (frames 5419 to 5422, 6540 to 6543, and 6271) and in

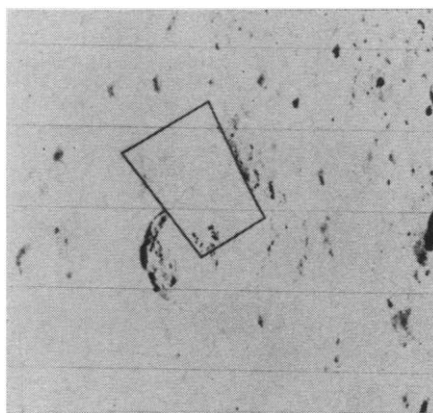


Fig. 1. Part of Lunar Orbiter I frame M-136 showing crater 211 (1) nearly in the center. Note the Y-shaped central peaks. A detail of the marked area is shown in Fig. 2.

high resolution (frames 6448 and 6449). Both missions provided stereoscopic coverage of the crater and its environs.

Distinct layering is displayed along the crater walls, where rock ledges protrude at several levels within the wall terraces. At the rim crest, the first ledge of rock is in evidence along the crenulations, as in the middle of the right hand edge of Fig. 2 (Apollo 10, frame 4350). At lower levels on the wall, discontinuous rock ledges could be traced for distances of 10 km or more. These ledges are indicative of horizontal bedding and are different in their setting and textural characteristics from material produced by slumping and mass wasting along the walls.

In the northern segment of the crater wall there are at least four different rock types (Fig. 2). These are distinguished by their setting, textures, structures, and relative brightness. The first rock type is shown in area A, Fig. 2. It represents a mantle of relatively young material of low albedo. This material appears identical to that which can be seen in a pool-like depression beyond the rim crest of the crater (A'). The latter is part of an extensive unit that covers a region of more than several thousand square kilometers, as seen in the photographs from Apollo 8 (3). The textures and structures displayed by this unit are reminiscent of those exhibited by terrestrial lava flows. Wrinkles on its surface are common, especially at the lower parts of a given topographic level. The flow fronts are convex downslope and appear to be the result of a gentle or slow flow of molten material that has moved from higher to lower ground. There is also evidence of collapsed pool surfaces, as in the upper left edge of Fig. 2. An alternative interpretation of this mantling material would be that it is a debris flow or rock glacier. However, the aforementioned criteria signify an extrusive volcanic origin, that is, a lava flow.

The second rock type (area B, Fig. 2) is characterized by a very high albedo. Its texture is clearly different from that displayed by the rest of the crater wall. The latter represents a third rock type, a typical segment of which is marked C in the same figure. The brightest segment of the wall (area B) is characterized by a great number of massive domical hills. These are separated by shallow furrows filled by darker, probably fine-grained, debris material. These features indicate that this segment of the crater wall is made